# Pore Dynamics of Lipid Vesicles Under Light-Induced Osmotic Stress

Vinit Kumar Malik,[1] On Shun Pak,[2] and Jie Feng[1,3,*]

[1] *Department of Mechanical Science and Engineering, University of Illinois at Urbana-Champaign, Urbana, Illinois 61801, USA*

[2] *Department of Mechanical Engineering, Santa Clara University, Santa Clara, California 95053, USA*

[3] *Materials Research Laboratory, University of Illinois at Urbana-Champaign, Urbana, Illinois 61801, USA*

(Received 23 March 2021; revised 4 September 2021; accepted 4 January 2022; published 10 February 2022)

Understanding the physical mechanisms governing the response of lipid vesicles under an osmotic imbalance is crucial not only for advancing our knowledge of osmoregulation in living cells but also for guiding the design of biomedical vesicular systems. When placed under osmotic stress, lipid vesicles exhibit a variety of responses, from simple engorgement, to swelling with eventual pore formation, to the only recently observed irreversible explosion triggered by photoreactions. Here, we present a unifying model that incorporates all of these dynamic responses by elucidating the associated energy landscape of vesicle outcomes. We demonstrate the essential, yet previously unrecognized, role of the spontaneous curvature in determining vesicle responses under extreme osmotic stress. We utilize numerical experiments to construct phase diagrams of pore dynamics, which are consistent with the experimental observations, and we further discuss the impacts of compositional lipid properties. Our work not only advances a fundamental understanding of vesicle response in nonequilibrium environments, but also extends the possibility for precise design of vesicle systems regarding controlled release of therapeutic substances in biomedical applications.

DOI: 10.1103/PhysRevApplied.17.024032

## I. INTRODUCTION

Vesicles, small compartments bounded by lipid bilayer membranes, have been widely considered as an essential rudimentary biophysical model for enriching our understanding of the origins of life [1] and the physiology of biological cells [2]. In cellular physiology, one widely encountered environmental assault on cells is osmotic stress, which may cause the cell to swell, rupture, and die [2]. Therefore, studying vesicle mechanical responses in a nonequilibrium osmotic environment is of general interest to the biophysics community, with an ultimate goal of mapping biological cell-membrane functions [3–8]. In addition, artificial biomembrane systems have recently been developed to leverage osmotically induced lysing in applications such as vesicle-based delivery of nutrients, biological actives, and pharmaceuticals [9–12].

Rudimentary giant unilamellar vesicles (GUVs) can respond in a number of ways to an osmotic imbalance, crucially depending on the degree of osmotic imbalance across the vesicle membrane as well as the vesicle size. Smaller vesicles achieve osmotic equilibrium by leaking their contents through a series of transient pores, while larger vesicles tend to open a long-lived pore to relax osmotic stress [13]. A classical form of the total energy of a vesicle $E = 2\pi\gamma R\sin\alpha + \sigma^2 A_0/2K$, which neglects bending energy, has been employed to model lipid vesicles' osmotic response [3–8,13–15]. The first term $2\pi\gamma R\sin\alpha$, represents the pore-edge energy, where $\gamma$ is the line tension of the lipid membrane, $R$ the vesicle radius, and $\alpha$ the angle subtended by the pore edge and vesicle center, respectively. The second term $\sigma^2 A_0/2K$, contributes to the elastic energy due to membrane stretching, as introduced by Helfrich [16]. Here, $K$, $\sigma$, and $A_0$ are the elastic stretching modulus of the lipid membrane, the membrane tension, and the initial area of the vesicle, respectively. Following the energy argument proposed by Lister [3], Taupin *et al.* [4] successfully explained osmotic-pressure-induced leakage in lipid vesicles, and Koslov and Markin [5] further predicted a swell-burst-reseal cycle as the most probable path for vesicle relaxation in an osmotic imbalance. Later, theoretical and experimental studies performed by Brochard-Wyatt and co-workers [6,7,17] established that vesicles relax following the release of inner contents by opening only a single pore. The pore-opening events in vesicles were presumably analogous to the opening of a hole in a viscous film. Using this model, Levin and Idiart [13,14] predicted the existence of short- and long-lived pores in lipid membranes under osmotic stress. However, not accounting for the aqueous viscosity

*jiefeng@illinois.edu

 

resulted in an unphysical value of approximately 100 Pa s for membrane internal viscosity, extracted by fitting the theoretical pore size to the available experimental data. Ryham *et al.* [18] resolved this discrepancy by incorporating the aqueous viscous dissipation in the governing equation of pore opening and showed that, in fact, the aqueous viscous dissipation dominates the internal membrane viscous dissipation. These modeling effects have been successfully employed to a variety of situations of vesicles under osmotic stress [8,15,19–21].

This classical model, however, cannot predict the disintegration of the vesicle membrane, i.e., a vesicle explosion, as observed in recent experiments [22,23]. It has been shown that, under an osmotic shock, vesicles can undergo irreversible bursting by disintegrating into several daughter structures [22,23], a hitherto unexplained regime of vesicle response to osmotic stress. Figure 1 shows the schematic of vesicle explosion aligned with experimental images from Zhu and Szostak [22]. We have previously demonstrated that a rapid and extreme osmotic imbalance, as generated by photochemical reactions, induces vesicle swelling at an acutely fast rate. The high loading rate associated with this rapid size expansion increases the lytic tension $\sigma_l$, causing the vesicle to grow a large pore and ultimately disintegrate. In addition, we highlighted the significance of the bending energy and spontaneous curvature in modeling vesicle explosion [24].

Prior work on closed vesicle shape transformations has shown the vital contributions of the bending energy in determining morphological outcomes [25,26]. This motivates us to consider how the bending energy might impact the phase diagram for open vesicle systems, such as a vesicle with a pore. The bending energy is related to the spontaneous curvature $H_s$ of the lipid membrane [16], which is defined as the preferred curvature of membranes in mechanically relaxed states [27]. $H_s$ arises due to asymmetric adsorption of solutes or different depletion layers across the membrane because of repulsive interactions between solutes and lipid membrane [28]. For instance, lyotropic ions or molecules, such as sucrose and glucose, can disrupt the hydrogen-bond network of water, causing the attractive or repulsive interactions with the membrane lipids [29]. Indeed, the photochemical reaction product bicarbonate ion $HCO_3^{-1}$, a known chaotrope [30], also present in vesicle explosion experiments [22], may disrupt the hydrogen-bonding network between water molecules and induce a spontaneous curvature. In particular, at high concentration differences like those generated with an active chemical reaction [24], the effect of the spontaneous curvature could become significant [31,32] and thus the bending energy should be taken into account. While prior work on open vesicles in a hypotonic environment has typically neglected the bending energy by assuming spontaneous curvature to be absent [4–8,13], we incorporate the contributions of the bending energy into our formulation of the total energy, and integrate vesicle exploding with the known swell-burst-reseal regime regarding the pore dynamics to produce a general framework applicable across a wide range of experimental parameters.

To systematically investigate different pore dynamics across vesicle sizes ranging from the nano- to microscale, we present a quantitative regime map, incorporating the previously unincluded explosion under hypotonic conditions. We show how the bending energy plays a crucial role in vesicle explosion. Taking this into account, we further establish a lower limit at which long-lived pores cease to exist. Additionally, we discuss the influence of different membrane properties—such as bending rigidity, elastic modulus, and the permeability coefficient—on the phase diagram of pore stability. In particular, we unravel the impact of chemical rate constants on vesicle response to an active osmotic gradient by showing the competition between the chemical reaction and swelling time scales of vesicles.

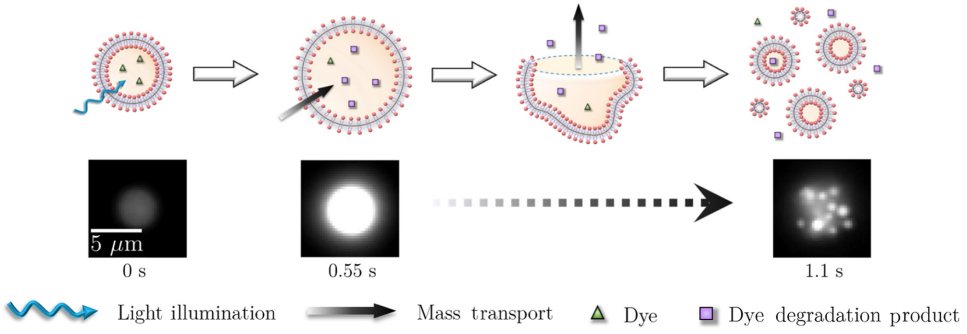


FIG. 1. Schematic illustrations of giant unilamellar vesicle explosion under light-induced osmotic stress (top row), with the corresponding experimental images showing different stages of explosion [22] (bottom row). Light illumination causes rapid decomposition of photosensitive solutes inside a vesicle. Due to an osmotic influx, the vesicle swells rapidly. The vesicle membrane ruptures once the membrane tension $\sigma \geq \sigma_l$ (lytic tension). If the pore becomes large enough, the vesicle enters the buckling regime, undergoing large membrane undulations and ultimately disintegrating into daughter structures.

## II. FORMULATION

We begin by modeling a vesicle with a single pore formation in a hypotonic environment. In our model, we consider the vesicle shape as a sphere even after the pore has opened. The assumptions of the spherical shape of a ruptured vesicle and the existence of only a single pore in a hypotonic solution are corroborated by previous experimental observations [6,7]. Figure 2 depicts a schematic of such a vesicle containing a single pore opening with an embedded coordinate system. The vesicle radius $R$ and the angle $\alpha$ (measure of pore size), constitute the configuration space. To derive the governing equations of vesicle dynamics under hypotonic conditions, we utilize the conservation principle of mass for solvent and solutes. In addition, the Lagrangian framework for nonconservative systems is used to develop the governing equation of pore growth.

### A. Stochastic membrane rupture

Previous experimental observations have demonstrated that membrane lytic tension, $\sigma_l$, follows a strain-rate-dependent probability distribution [33,34]. To model this stochasticity and the strain-rate dependence of membrane rupture, we adopt the formulation of a survival probability $S(t)$, following Evans and Smith [34], as a first-order kinetic rate equation given by

$$\frac{dS(t)}{dt} = -k_{\text{hole}} S(t), \tag{1}$$

where $k_{\text{hole}}$ is the frequency of appearance of an unstable initial prepore, which has the potential to subsequently form a pore. $k_{\text{hole}}$ is given by

$$k_{\text{hole}} = \frac{k_\delta e^{\sigma/\sigma_\delta}}{\left(1 + e^{(\sigma_\beta/\sigma)[1-(\sigma r_\delta/\gamma)]^2}\right)}. \tag{2}$$

The parameters $k_\delta$ and $r_\delta$ used to evaluate $k_{\text{hole}}$, are the preexponential frequency factor, and the mean radius of symmetry breaks, respectively [34]. $\sigma_\delta = k_B T/\pi r_\delta{}^2$ is a surface tension scale set by $r_\delta$, while $\sigma_\beta = \pi\gamma^2/k_B T$ is a thermal tension scale set by $\gamma$. A typical range of $k_\delta$ and $r_\delta$ for phosphatidylcholine (PC) bilayers are $k_\delta = 0.005 - 4$ Hz and $r_\delta = 0.4 - 1.5$ nm [33,34]. We use $k_\delta = 0.04$ Hz and $r_\delta = 0.42$ nm in the following discussion. We sample $t_l$, the moment of membrane rupture, from $S(t)$ using a Monte Carlo sampling approach to combine the kinetics of membrane rupture and subsequent pore dynamics.

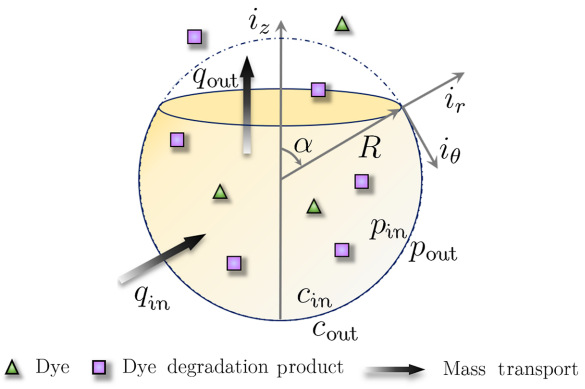


FIG. 2. Model setup for a spherical vesicle with an embedded circular pore. The radius of vesicle $R$ and the angle $\alpha$ subtended by a pore at the center of the vesicle provide a configuration space with a spherical coordinate system. Here $q_{\text{in}}$ and $q_{\text{out}}$ denote, respectively, mass transport in and out of the vesicle, and $\Delta p = p_{\text{in}} - p_{\text{out}}$ represents the pressure jump across the membrane.

### B. Pore dynamics

To model the pore growth, once the membrane has ruptured, we make use of Helfrich's spontaneous curvature-elasticity framework [16]. Thus, we write the total energy $E$ of the vesicle system as

$$E = 2\pi\gamma R\sin\alpha + \frac{\sigma^2}{2K}A_0 + \frac{1}{2}k_b\int_A (H - H_s)^2\, dA - \int_{R_0}^{R} \Delta p\, 2\pi R^2(1+\cos\alpha)\, dR. \tag{3}$$

At the right-hand side of Eq. (3), we incorporate the membrane bending energy as the third term. Here, $k_b$ represents the membrane bending rigidity. The work done by pressure is incorporated as the fourth term [24]. We recognize that work done by pressure has been included in prior models to describe vesicle dynamics in hypotonic environments [35]. Note that Eq. (3) could be interpreted as a generalized potential [36] under an external force, e.g., as proposed in the case of microtubule formation when the membrane is pulled by a point force [37]. In addition, the work done by excess pressure $\Delta p$ across the membrane is only nonzero when there is a change in vesicle radius $R$. As the $\Delta p$ changes with the radius $R$, this work done has been expressed in an integral form. Since the vesicle osmotic response dynamics depends only on the gradient of the total energy $E$, the gradient of the work done by $\Delta p$ is independent of $R_0$, the initial radius of the vesicle.

For a spherical vesicle, $H = 2/R$ is the instantaneous curvature. In our system, solute concentration asymmetry between the inner and outer environments gives rise to the spontaneous curvature, $H_s$. This increases the significance of the bending-energy contributions to the total energy of vesicle in the case of a large pore [24]. As established in previous studies [31,32], we adopt a linear relationship between the spontaneous curvature $H_s$ and

the concentration difference across the membrane, $\Delta c$, as it accommodates both modes of spontaneous curvature generation by asymmetric adsorptions as well as formation of asymmetric depletion layers across the membrane [38]. Therefore, $H_s$ is coupled with $\Delta c$ and will evolve as the chemical reaction progresses. Specifically, we use $H_s = \beta \Delta c$, with $\beta$ as a constant of proportionality. Here, $\beta$ is related to the strength of the molecular interaction with the lipid membrane as well as membrane bending rigidity $k_b$. Assuming an average molecular size of 0.5 nm (e.g., the size of a glucose molecule is 0.6 nm) and a membrane thickness of $d = 4$ nm, $|\beta|$ is estimated to be in a range between 0.006–0.03 $\mathrm{M}^{-1}\,\mathrm{nm}^{-1}$ [31,38]. In our simulations, unless stated otherwise, we use a constant $\beta = -0.005\ \mathrm{M}^{-1}\,\mathrm{nm}^{-1}$ (a negative sign signifies that the membrane bends locally away from the inner compartment, consistent with the sign convention used by Lipowsky [28]). Even for a maximum $\Delta c_0 = 10$ M considered in this work, the maximum spontaneous curvature generated is $|H_s| = 0.05\ \mathrm{nm}^{-1} < 1/d = 0.25\ \mathrm{nm}^{-1}$ and still within the practical range as shown in prior work [32].

As the pore grows, the viscous forces in both the membrane and the surrounding fluid dissipate the energy. To model the dissipation experienced by the growing pore, we formulate the damping using a Rayleigh dissipation function [36,39] as

$$\Phi = \pi C_1 \eta_s R \sin\alpha R^2 \dot{\alpha}^2 + 2\pi C_2 \eta_m d R^2 \dot{\alpha}^2, \tag{4}$$

where the first term on the right-hand side corresponds to dissipation in the aqueous solution, while the second term corresponds to membrane internal dissipation. Here $C_1$ and $C_2$ are geometric coefficients derived from a detailed flow-field analysis [15]. $\eta_s$, $\eta_m$, and $d$ are solvent viscosity, membrane viscosity, and membrane thickness, respectively. The overhead dot $\dot{(\,)}$ represents the time derivative.

Now we can follow the Lagrangian framework [15,36] for Eqs. (3) and (4). The governing equations for the evolution of the vesicle system are

$$\frac{1}{R}\frac{\partial E}{\partial \alpha} = -\frac{\partial \Phi}{\partial (R\dot{\alpha})}, \tag{5a}$$

$$\frac{\partial E}{\partial R} = -\frac{\partial \Phi}{\partial \dot{R}}. \tag{5b}$$

Following Eq. (5a), we obtain the governing equation for pore evolution as

$$\begin{aligned}\Big(C_1 \eta_s R \sin\alpha + 2C_2 \eta_m d\Big)\dot{\alpha} \\ = \Big[ -\frac{\gamma \cos\alpha}{R} - \frac{2\sigma R_0^2}{KR^2}\frac{\partial \sigma}{\partial \alpha} + \frac{1}{2} k_b (H - H_s)^2 \sin\alpha \Big] \\ \times \theta(t - t_l).\end{aligned} \tag{6}$$

Here, we use the Heaviside function to incorporate the stochasticity of membrane rupture, such that the membrane remains intact until the sampled time $t_l$ (i.e., $\dot{\alpha} = 0$ for $t < t_l$). Additionally, using Eq. (5b), we obtain the governing relation for excess pressure as

$$\begin{aligned}\Delta p = \frac{\gamma \sin\alpha}{R^2\,(1 + \cos\alpha)} + \frac{2\sigma R_0^2}{KR^2\,(1 + \cos\alpha)}\frac{\partial \sigma}{\partial R} \\ + k_b \left( \frac{H_s^2}{R} - \frac{2H_s}{R^2} \right).\end{aligned} \tag{7}$$

Here, the pressure jump across the membrane is not only caused by the membrane tension, but also from the pore-edge energy and membrane-bending energy. Equation (7), under the assumptions of the classical model, which includes only pore-edge energy and membrane-stretching energy, can be reduced to a classical excess Laplace pressure as $\Delta p = 2\sigma/R$. Moreover, we note that Eq. (7) can be derived following the principle of virtual work as in Refs. [40,41].

To compute $\partial\sigma/\partial R$ in Eq. (6) and $\partial\sigma/\partial\alpha$ in Eq. (7), we define the membrane tension $\sigma$ using the constitutive relation described in Ref. [42] such that

$$\frac{A}{A_0} - 1 = \frac{k_B T}{8\pi k_b} \ln\left(1 + \frac{\sigma A}{24\pi k_b}\right) + \frac{\sigma}{K}. \tag{8}$$

Here, $A = 2\pi R^2(1 + \cos\alpha)$ is the vesicle surface area, $k_b$ is the bending rigidity of the membrane, and $k_B T$ is the thermal energy scaling factor. The first term on the right-hand side of Eq. (8), represents the flattening of membrane undulations, which mostly preserves the area per lipid molecule. However, the second term accounts for the direct stretching of the membrane. It has been shown that under compression, the membrane tension reaches a small negative plateau value. In compression, the membrane prefers bending, which reveals the buckling of the membrane [43,44]. The onset of buckling is predicted by Eq. (8) for $\sigma \approx -24\pi k_b/A_0$ where the first mode of the thermal undulations become unbounded [44].

### C. Mass transport across vesicle membrane

In addition to pore dynamics, we further consider mass transport of the solute and solvent across the vesicle membrane. This is motivated by the observation that the vesicle volume changes because of the osmotic influx across the membrane and leakout through the pore. The osmotic influx results from two competitive pressures—the osmotic pressure driven by the solute differential $\Delta c = c_{\mathrm{in}} - c_{\mathrm{out}} > 0$, and the pressure jump $\Delta p$ in Eq. (7), and thus is written as $q_{\mathrm{in}} = P\nu_s(\Delta c - \Delta p/R_G T)$. Here, $P$ is the permeability coefficient, $\nu_s$ is the solvent molar volume, $R_G$ is the universal gas constant, and $T$ is

temperature. On the other hand, the outflux of inner contents through the pore, in a low Reynolds number regime, can be described as $q_{\text{out}} = \Delta p R \sin\alpha / Q\eta_s$ where $\eta_s$ is the solvent viscosity and $Q$ is a geometric coefficient accounting for the finite spherical geometry of the vesicle [15]. Therefore, mass conservation of the solvent is governed by

$$\frac{dV}{dt} = q_{\text{in}}A - q_{\text{out}}A_p. \tag{9}$$

Here, $V = (\pi/3)R^3\left(2 + \frac{9}{4}\cos\alpha - \frac{1}{4}\cos 3\alpha\right)$, $A = 2\pi R^2(1+\cos\alpha)$, and $A_p = \pi R^2 \sin^2\alpha$ is the vesicle volume, surface area, and circular pore area, respectively. By substituting $V$ in Eq. (9), we formulate the time rate of change of vesicle radius $R$ as

$$\left(A + A_p\cos\alpha\right)\dot{R} = q_{\text{in}}A - \left(q_{\text{out}} - R\dot{\alpha}\sin\alpha\right)A_p. \tag{10}$$

Next, the mass conservation of solute molecules is governed by the phototriggered chemical decomposition, the diffusion and convection of solution through the pore, which gives the governing equation as follows:

$$\frac{d(V\Delta c)}{dt} = VZkc_{\text{sub}} - q_{\text{out}}A_p\Delta c - \frac{D}{R}A_p\Delta c, \tag{11}$$

where $Z$, $k$, $c_{\text{sub}}$, and $V$ are, respectively, the net stoichiometric coefficient, the chemical rate constant, the substrate concentration, and the vesicle volume. $D$, the diffusion constant of the solute, is estimated as the diffusion coefficient of sucrose ($D_{\text{solute}}$ as noted in Table I). In writing Eq. (11), we presume that the chemical reaction is occurring in a spatially uniform manner and that it follows first-order kinetics [24]. The first term, $Zkc_{\text{sub}}$, on the right-hand side of Eq. (11), represents the contribution occurring from the generation of solute moles. The second term constitutes the loss of solute via bulk mass transport out of the vesicle, while the third term accounts of diffusive loss of the solute through the circular pore. Now, using the product rule of derivatives and substituting $dV/dt$ from Eq. (9), we obtain

$$\frac{d\Delta c}{dt} = Zkc_{\text{sub}} - \frac{\Delta c}{V}\left(q_{\text{in}}A + \frac{D}{R}A_p\right). \tag{12}$$

The coupled equations, Eqs. (1), (6), (10), and (12), constitute our model for vesicle dynamics. Equations (1) and (6) control the membrane rupture and pore growth dynamics, while Eqs. (10) and (12) govern the continuum mass transport across the vesicle as well as contributions from the chemical reaction. To obtain the vesicle dynamics under osmotic imbalance, we solve Eqs. (1), (6), (10), and (12) numerically. We compute the excess pressure $\Delta p$, and membrane tension $\sigma$ using Eqs. (7) and (8), respectively, which depends only on the configuration state, at the current time step. We note that a validation study performed in our previous work [24] shows good agreement between the model predictions and experimental results regarding the time period of swell-burst-reseal cycles reported by Chabanon *et al.* [8]. In the current work, the parameter values used in the numerical experiments are representative of PC bilayers, as listed in Table I.

TABLE I. Characteristic values for the physical parameters used in the simulation.

| Parameters | Values | References |
|---|---|---|
| $d$ | 3.5 nm | [42] |
| $v_s$ | $18.04 \times 10^{-6}$ m$^3$/mol | [8] |
| $\eta_s$ | 0.001 Pa s | [8] |
| $\eta_m$ | $5 \times 10^{-9}$ Pa s | [45] |
| $D_{\text{solute}}$ | $5 \times 10^{-10}$ m$^2$/s | [46] |
| $\gamma$ | 8.6 pN | [47] |
| $k_b$ | $6 \times 10^{-20}$ J | [42] |
| $K$ | 0.15 N/m | [42,48] |
| $P$ | 50 $\mu$m/s | [49] |
| $r_\delta$ | 0.42 nm | [33,34] |
| $k_\delta$ | 0.04 Hz | [33,34] |

## III. RESULTS AND DISCUSSION

### A. Energy landscape

To investigate the stability of the system, we first analyze the evolution of the total energy $E$ of the vesicle as the pore angle $\alpha$ grows. Using Eq. (3) for a constant $R/R_0 > 1$, we show the typical evolution of the total energy of a vesicle with $\alpha$ in Fig. 3(a). As the pore grows, the vesicle membrane relaxes, lowering the total energy $E$. Figure 3(a) reveals two stationary points, $\alpha_a$ and $\alpha_b$ of an energy profile with respect to $\alpha$. For smaller $R/R_0$, the pore grows up to the first stationary point, $\alpha_a$. Between $\alpha_a$ and $\alpha_b$, the pore-edge energy dominates the bending energy, imposing an energy barrier. The growing pore then experiences an adverse energy gradient causing it to reseal. At the second stationary point $\alpha_b$, most of the stretching energy has relaxed, leaving only the bending and pore-edge energy to compete. However, beyond $\alpha_b$, the bending energy begins to dominate, curving the energy profile downwards and creating favorable energy gradient for larger $\alpha$. As in the case for larger $R/R_0$, if the pore grows larger than $\alpha_b$, the vesicle keeps unfolding until it buckles. By increasing $R/R_0$, as shown in Fig. 3(a), the difference between $\alpha_a$ and $\alpha_b$ decreases and finally merge. We refer to this configuration $(R/R_0, \alpha)_{\text{cr}}$ as the critical configuration, where the energy barrier between $\alpha_a$ and $\alpha_b$ vanishes. The conditions of critical configuration $(R/R_0, \alpha)_{\text{cr}}$ are given by $\partial E/\partial\alpha = 0$ and $\partial^2 E/\partial\alpha^2 = 0$. Once the vesicle attains this critical configuration, pore growth become unbounded, leading the vesicle to eventual disintegration into multiple daughter structures.

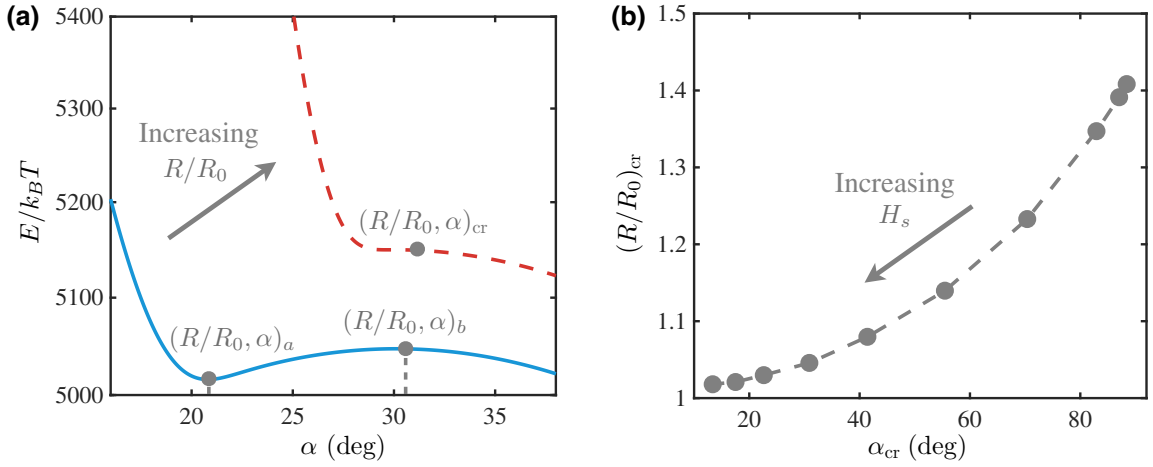


FIG. 3. Energy landscape and critical configuration of an osmotically stressed vesicle with a pore formation ($R_0 = 0.1$ $\mu$m). (a) Typical energy profile ($H_s = 0.05$ nm$^{-1}$) of a vesicle as the pore grows at constant $R/R_0$. $\alpha_a$ and $\alpha_b$ are the stationary points with respect to $\alpha$. (b) Dependence of critical configuration $(R/R_0,\alpha)_{\rm cr}$ on the induced spontaneous curvature $H_s$ due to asymmetric solute concentrations across the vesicle membrane. The values of relevant parameters are listed in Table I.

As the induced spontaneous curvature $H_s$ increases, so does its contribution in the bending energy. The critical configuration reveals the dominance of the bending energy, given that it is mainly affected by the spontaneous curvature $H_s$. At a higher asymmetry of inner and outer concentration, the induced spontaneous curvature is significant enough that the bending energy of the membrane becomes comparable in magnitude to the membrane-stretching energy. Figure 3(b) shows the dependence of the critical configuration on the induced spontaneous curvature $H_s$. When the induced spontaneous curvature $H_s$ increases (i.e., at higher degrees of asymmetry in concentrations across the vesicle membrane), the critical configuration becomes less stringent in the sense that it moves towards the initial configuration $(R/R_0,\alpha)_{\rm cr} = (1, 0)$. We can then infer that at higher osmotic stress the vesicle is more likely to explode as soon as it ruptures.

Next, to show how a pore evolves in an osmotically stressed vesicle, we present the dynamics of the pore radius under three different hypotonicity conditions ($\Delta c =$ 0.1, 0.4, and 1.5 M) as shown in Fig. 4. Figure 4(a) shows the pore evolution while in Figs. 4(b)–4(d) we plot the vesicle dynamics in the configuration space $R/R_0$—$\alpha$. For a short-lived pore, as shown in Fig. 4(b), it completes a closed loop, indicating resealing of the pore. This loop represents the characteristic response of a vesicle as a series of swell-burst-reseal cycles. For long-lived pores, the pore maintains an equilibrium size near the closure of the pore, settling at an equilibrium configuration with an open pore instead of completing the loop [Fig. 4(c)]. An exploding vesicle, however, buckles as the pore grows so large that it enters the buckling regime [Fig. 4(d)], with a consequent disintegration into daughter structures.

Although the bending energy plays a crucial role at larger pore sizes, historically it has been neglected in modeling pore dynamics in nonequilibrium osmotic environments [4–8,13]. In earlier models, once the vesicle membrane is relaxed by the opening of a pore, it leaves only the pore-edge energy, driving the pore closure, therefore no explosion event is even likely. In reality, at large $\alpha$ and $H_s$, the bending energy alters the curvature of the total energy, signifying its dominance over the pore-edge energy, causing the pore to grow large and ultimately resulting in vesicle buckling. Therefore, consideration of the bending energy is vital to integrate explosion with other known pore dynamics. Meanwhile, another factor influencing the vesicle response is the dependence of membrane lytic tension $\sigma_l$ on the swelling rate of the vesicle. Higher loading rates makes the lipid bilayers rupture at a higher strain [33,34]. As shown in Fig. 4(d), higher rupture strains lead to increased likelihood of vesicle explosion.

We further compare our model predictions [Figs. 4(e) and 4(f)] against the experimentally observed vesicle explosion [22]. In plotting Figs. 4(e) and 4(f), we choose the parameters as $\beta = -0.013$ M$^{-1}$ nm$^{-1}$, $k_\delta = 0.023$ Hz, and $r_\delta = 0.42$ nm, which predict the similar swelling time, and rupture strain as observed in experiments [22]. From the available experimental data of the vesicle-swelling phase, we obtain the relevant parameters $Z$ and $k$ [24] for Eq. (12). Figure 4(e) presents the simulated vesicle dynamics, with experimental parameters of all available cases in prior work [22], in $R/R_0 - \alpha$ configuration space. We note here that the rupture strain for all of the five vesicles is similar to experimental observations. All these vesicles grow a large pore and enter the buckling regime shown as the

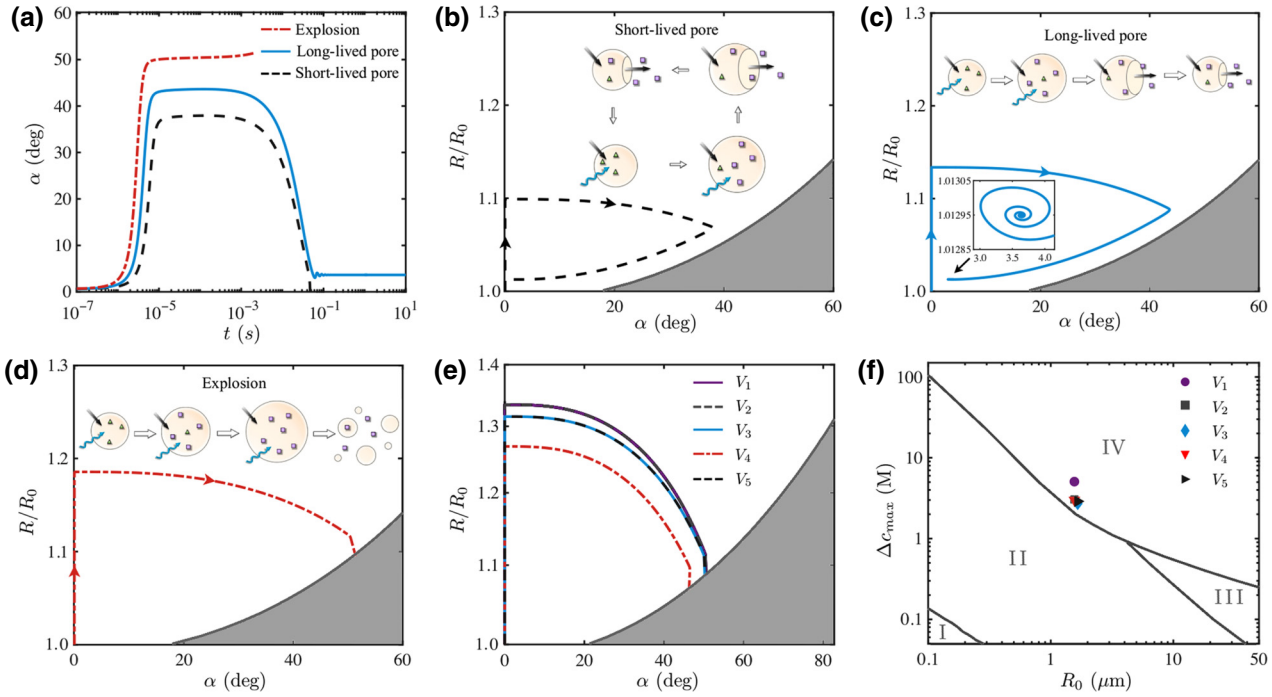


FIG. 4. Pore dynamics of an osmotically stressed vesicle with an initial radius $R_0 = 5\ \mu$m, and experimental comparison of vesicle explosion. (a) Evolution of pore in time. The dashed, solid, and dash-dot curves show the short-lived pore, long-lived pore, and explosion under increasing osmotic stress with $\Delta c = 0.1, 0.4$, and 1.5 M, respectively. (b) Short-lived pore dynamics forming a loop in the configuration space. The gray shaded area indicates the buckling regime. (c) Long-lived pore dynamics showing the vesicle approaching an equilibrium state. Inset shows the oscillations around the equilibrium state. (d) Explosion event. The intersection of the pore dynamics with the buckling regime indicates occurrence of membrane disintegration. The values of relevant parameters are listed in Table I. (e) Comparison of pore dynamics with experiments of vesicle explosion. The curves show the simulated explosion dynamics of vesicles response, where $V_i$ represents the $i$th vesicle. (f) Phase diagram of vesicles under light-induced osmotic imbalance. The markers show theoretically predicted vesicles response, where $V_i$ represents the $i$th vesicle. The boundaries, solid gray curves, between different regimes are plotted for an average chemical rate constant $k = 5.07\ 1/\text{s}$ of the five vesicles extracted from experiments [22].

shaded gray area, subsequently disintegrating into smaller daughter structures. Thus, the comparison shows that our model predictions are consistent with the experimental results.

Meanwhile, to better quantitatively map the regimes of vesicle osmotic responses, we present the phase diagram in $\Delta c_{\max} - R_0$ phase space where $\Delta c_{\max} = Z c_{\text{sub}_0}$. Here, $c_{\text{sub}_0}$ represents the initial concentration of a substrate encapsulated inside vesicles. To plot such a phase diagram, we perform numerical experiments solving Eqs. (1), (6), (10), and (12) simultaneously for different configurations. As shown in Fig. 4(f), we identify four regimes regarding the pore dynamics. Regime I indicates no pore being formed under the given osmotic imbalance. Physically, given the smaller size of the vesicles in regime I and the inverse relationship of excess pressure $\Delta p$ with the vesicle size, even a small level of swelling will generate enough pressure to balance the osmotic pressure without causing the membrane to rupture. For the mid-size vesicles (i.e., those represented in regime II), formation of a series of short-lived pores comprises the well-known response to an osmotic imbalance adopting a characteristic swell-burst-reseal cycle. However, vesicles in regime III open a stable long-lived pore under osmotic stress. Finally, regime IV represents the extreme event of vesicle explosion. In this regime, a vesicle that attains the critical configuration $(R/R_0, \alpha)_{\text{cr}}$ explodes. It is worthwhile to note here that regime III vanishes at extreme osmotic stress—i.e., high $\Delta c$. This exhibits a scenario in which there is competition only between the stretching energy and bending energy. At an extreme osmotic imbalance, due to a large induced spontaneous curvature $H_s$, the contribution of the bending energy is comparable to stretching energy. The gray solid phase boundaries between each regime are plotted for an average chemical rate constant $k$ of five vesicles extracted from experiments [22]. We map the five experimental cases on the phase diagram and show that the vesicles lie in the predicted explosion regime. Therefore, we can infer, from Fig. 4(f), that the model predictions align well with the observed experimental exploding. We note that we do not realize any prior work showing regime IV for pore dynamics. Therefore, via the general model

presented in this work, which takes into account both the bending energy and lytic tension, we are able to capture all experimentally observed vesicle responses to differing amounts of hypotonicity in nonequilibrium environments.

### B. Phase diagrams

To provide engineering design guidelines across a wide range of parameters, we explore the impact of key lipid membrane properties such as $k_b$, $K$, and $P$ on the boundaries of the phase diagrams (Fig. 5). We focus on these properties as $k_b$ and $K$ influence the bending and elastic energies of a vesicle, while $P$ predominantly changes the vesicle swelling rate—all of which are factors in determining the vesicle response to an osmotic gradient. Moreover, these properties can be manipulated within a wide range, by changing the composition of the lipid bilayer such as moderating the fraction of cholesterol lipids during vesicle fabrication. In particular, prior work shows that the bending rigidity $k_b$ of lipid membranes typically ranges from 10–60$k_BT$ [42,50], and could be altered up to threefold, for, e.g., by incorporating cholesterol [51] or by manipulating the salt concentration of the surrounding aqueous environment when using charged lipid membranes [52]. In our simulations, bending rigidity ranges from $k_b \approx$ 15–45$k_BT$. On the other hand, the stretching modulus $K$ varies in between $K \approx$ 100–300 mN/m [42,50,53], and a similar range for Fig. 5(b) is considered in simulations. For Fig. 5(c), we use a value of the permeability coefficient ranging between $P =$ 10–100 $\mu$m/s as has been observed in experiments [49]. In addition, we consider the vesicle with a size of 100 nm–50 $\mu$m, which covers the typical size range produced with various experimental techniques [54]. We construct the phase diagram of

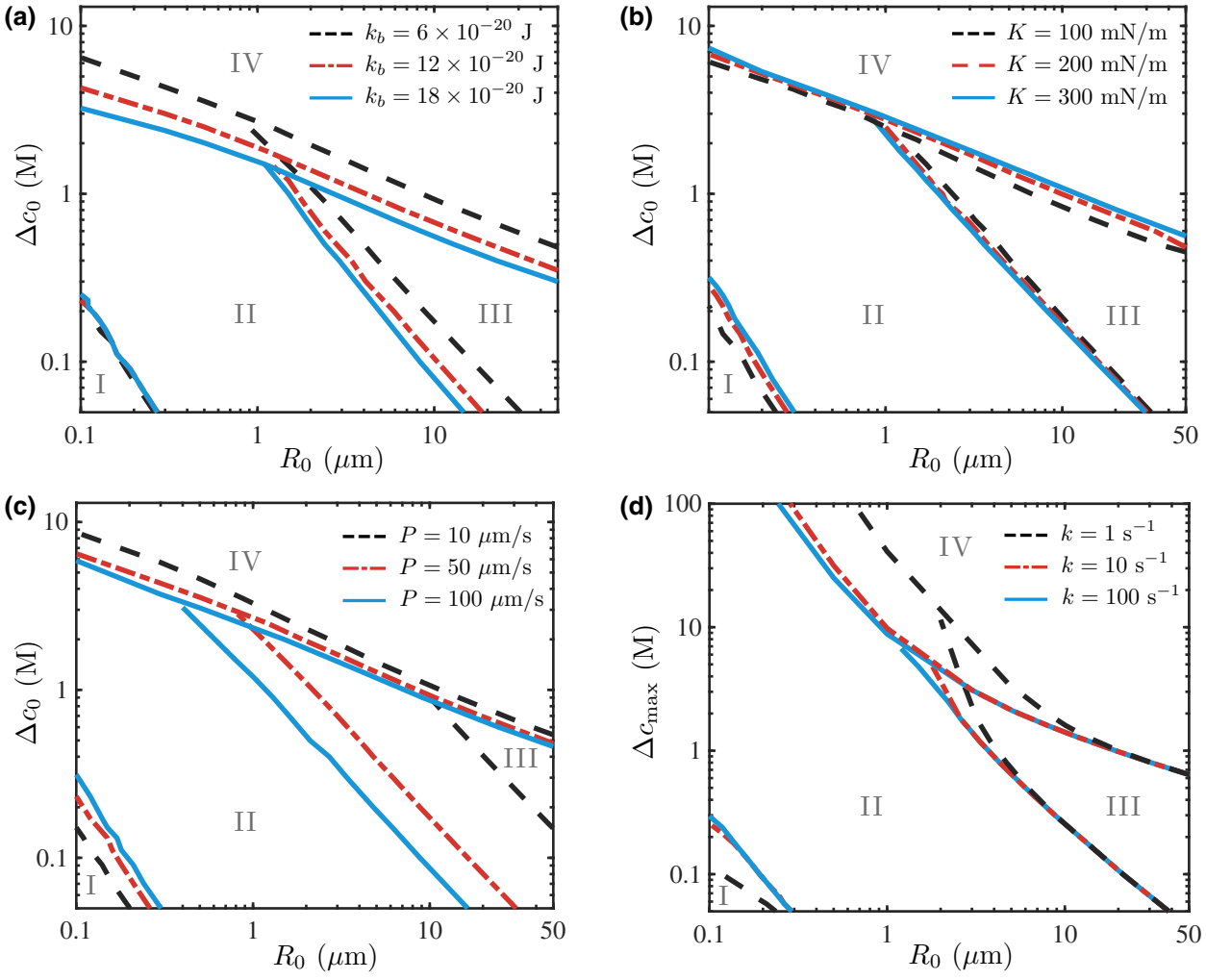


FIG. 5. Phase diagrams of a vesicle under hypotonic conditions for different values of (a) bending rigidity of the membrane, $k_b$. (b) Elastic modulus of the membrane, $K$. (c) Permeability coefficient, $P$. (d) Chemical reaction rate constant, $k$. Here, regime I: the vesicles remains intact (no pore formation); regime II: formation of short-lived pores; regime III: the long-lived pore; regime IV: vesicle disintegration into daughter structures. The values of relevant parameters are listed in Table I, except indicated in the figure.

vesicle responses in a phase space of $\Delta c - R_0$. In plotting these phase diagrams, we perform numerical experiments solving Eqs. (1), (6), and (10) simultaneously for different configurations in the $\Delta c - R_0$ phase space with $d\Delta c/dt = 0$. We consider constant $\Delta c$ due to the following: (1) such a system can be realized for vesicles with an internal chemical reaction; (2) changes in the concentration difference across the membrane are typically much slower than the time scale of pore growth and collapse [8,13].

Figure 5(a) shows the impact of bending rigidity $k_b$, on the phase boundaries of vesicle responses under an osmotic imbalance. The lipid bilayers are extremely compliant to bending, owing to very small values of $k_b$ (of the order of few tens of $k_BT$ [42,50]), thus it does not play a significant role during the swelling or initial pore growth phase. We note, in Fig. 5(a), that the phase boundary of regime I is not affected as the mechanical response is dominated by the membrane elastic energy. However, the membrane elastic energy is relaxed in regimes III and IV, and the significance of the bending energy increases to counter the pore-edge energy in resealing the membrane. As shown in Fig. 5(a), the phase boundaries between regimes II and III, and IV are altered significantly. As the membrane becomes more resistant to bending, the bending energy effectively counters the pore-edge energy, therefore the boundaries shift towards the origin, expanding the long-lived pore regime III and exploding regime IV. This behavior establishes the significance of the bending energy in modeling the vesicle's osmotic response. Given the membrane-bending rigidity of only tens of $k_BT$, it may not be immediately apparent that there exists such a regime where the bending energy is dominating the vesicle's response. However, for a large spontaneous curvature $H_s$, such as in the present case of a large concentration difference, $\Delta c$, and asymmetric vesicles (composed of different inner and outer leaflets) [55,56], the bending energy would become essential for accurately modeling vesicle lysis.

On the other hand, Fig. 5(b) demonstrates that the membrane elastic modulus $K$, does not alter the phase boundaries significantly. The vesicle loading rate depends on the elastic modulus as $\dot{\sigma} \propto K\dot{\varepsilon}_a$. Meanwhile, the membrane tension, generated due to swelling, is also directly proportional to $K$. As $K$ increases, the loading rate increases, making the membrane rupture at a higher membrane lytic tension $\sigma_l$; however, with increased $K$, the membrane lytic tension can be achieved at lower area strain. The mild impact of membrane-stretching modulus $K$ on the vesicle dynamics results from two counteracting effects: increasing the membrane loading rate $\dot{\sigma}$, and reducing the membrane area strain $\varepsilon_a$ at rupture.

The permeability coefficient of the membrane $P$ is expected to influence the membrane lytic tension $\sigma_l$, because the vesicle loading rate is directly proportional to the swelling rate as $\dot{\sigma} \propto \dot{R} \propto P\nu_s\Delta c/R_0$. As shown in Fig. 5(c), regime I expands away from the origin when the membrane becomes permeable, indicating that more permeable vesicles are capable of tolerating higher osmotic imbalance. Along the boundary between regime II and III, the pore maintains an equilibrium size governed by $q_{\text{in}} = P\nu_s\Delta c/R_0 = \Delta pR\sin\alpha/Q\eta_s = q_{\text{out}}$. By increasing the permeability coefficient $P$, the equilibrium can be maintained at a smaller $\Delta c$ as exemplified by the trend in Fig. 5(c). For regime IV, the higher the permeability, the higher the loading rate, hence the vesicle will rupture at a higher strain. Therefore, vesicles comprising more permeable membranes are more likely to explode under a given osmotic imbalance, as regime IV expands towards the origin [Fig. 5(c)].

To investigate how phototriggered chemical reactions can be harnessed for control over vesicle content release, we present the impact of the chemical rate constant on the vesicle response to an internally generated active osmotic gradient as shown in Fig. 5(d). We plot the phase diagram in $\Delta c_{\text{max}} - R_0$ phase space. An exemplar chemical rate constant, in the case of phototriggered chemical reactions, is $k \approx 10$ 1/s, which was inferred from previous experimental work [22,24]. Therefore, we choose $k = 1, 10$ and 100 1/s, which span a range of three orders of magnitude. As shown in Fig. 5(d), regime I boundary shifts away from the origin for a smaller reaction rate constant, as higher $\Delta c_{\text{max}}$ would be required to compensate for a slower chemical reaction. The boundary between regime II and III shows pronounced deviation from a straight line [as seen in Figs. 5(a)–5(c)] curving upwards for smaller vesicle sizes, and a similar trend for the boundary of the exploding regime IV is also observed. The influx time scale $R_0/P\nu_s\Delta c_{\text{max}}$ scales with the vesicle initial radius $R_0$. For smaller vesicles, $R_0/P\nu_s\Delta c_{\text{max}} \ll 1/k$, the vesicle swells quickly with not enough time for the chemical reaction to complete. Therefore, the vesicle membrane ruptures when only a small fraction of chemical reaction has been completed. Even if in general, higher permeability increases the chances of a vesicle exploding, the higher permeability with slower osmotic buildup may ultimately prevent explosion. This view aligns with previous observations of vesicles with higher permeability being less likely to explode [23] once the rate of osmotic change is accounted for. In such cases, the slow chemical reactions of these experiments drive the vesicles to enter a swell-burst-reseal regime.

In the present model, we do not consider the changes in the composition of the lipid membrane due to phototriggered products generated during the chemical reaction or the lipid damage caused by temperature generated by light exposure. The control experiments performed by Zhu and Szostak [22] show that the explosion of the vesicle was mainly attributed to the induced osmotic imbalance by phototriggered chemical reaction, and they ruled out the contribution of lipid membrane damage from the

photochemistry and temperature increase from illumination. Another potential limitation of the model is the assumption of a linear relationship of spontaneous curvature $H_s$ with $\Delta c$, which may not hold for the entire range of $\Delta c$ encountered in experiments. Additionally, while the line tension $\gamma$ may change due to the addition of molecules in the pore edge [7], we consider $\gamma$ as a constant.

## IV. CONCLUSION

In this study, we present a comprehensive model for pore dynamics of the vesicle response to a hypotonic osmotic gradient. This model could be extended to other processes generating an osmotic imbalance, such as active solute transports or metabolic activities by adapting the equation of mass conservation for solute. We further utilize numerical experiments to construct phase diagrams of the pore dynamics. Of note, we account for the exploding regime which was absent in previous studies. To account for systems of asymmetrical solute concentration, we consider the impact of an induced spontaneous curvature, which significantly alters the contribution of the bending energy. We demonstrate that it is imperative to account for the bending energy at large pore sizes as a driver of vesicle explosion. In the course of constructing an expanded phase diagram, strain at rupture also emerges as a key factor affecting vesicle outcomes. Vesicles that rupture at higher strain, tend to develop larger pores, causing the vesicle to explode. Vesicles with a membrane more rigid to bending or those that are more permeable are more likely to explode. We note that, the elastic modulus does not affect the vesicle responses significantly due to its counterbalancing effects on the vesicle loading rate and membrane lytic tension. In the case of an active osmotic gradient, the effect of a chemical rate constant is crucial with respect to the vesicle size. With smaller vesicle sizes, the swelling time scale is much shorter than the rate of chemical reaction, causing explosion to become unlikely.

By outlining key system properties that shift the phase boundaries of vesicle osmotic response, our work holds promise to aid in strategizing the release rate of vesicle's inner contents. The ability to rapidly release vesicle contents opens the possibility of engineering vesicles for precision drug delivery, such as targeted delivery of cancer chemotherapy medicines. Furthermore, it could serve as a first step towards designing multicompartmentalized cell mimetic systems with reaction cascades occurring in a spatiotemporally controlled manner, which may further contribute to understanding the osmosensing and enzymatic functions of living cells. Additionally, interactions of lipid membranes and proteins have been shown to induce local spontaneous curvature [57,58]. Such an induced spontaneous curvature may cause the membrane to rupture and form nanopores [59,60]. Therefore, our model may also provide perspectives about the role of the spontaneous curvature in the formation and stabilization of nanopores via pore-forming proteins, which has been crucial for defense and attack strategies in many organisms as well in the process of regulated cell death via membrane permeabilization.

## ACKNOWLEDGMENTS

J.F. was partially supported by American Chemical Society Petroleum Research Fund under Grant No. 61574-DNI9. O.S.P. was partially supported by NSF under Grant No. EFMA-1830958.

[1] K. Nishimura, T. Matsuura, T. Sunami, S. Fujii, K. Nishimura, H. Suzuki, and T. Yomo, Identification of giant unilamellar vesicles with permeability to small charged molecules, RSC Adv. **4**, 35224 (2014).
[2] E. K. Hoffmann, I. H. Lambert, and S. F. Pedersen, Physiology of cell volume regulation in vertebrates, Physiol. Rev. **89**, 193 (2009).
[3] J. D. Litster, Stability of lipid bilayers and red blood cell membranes, Phys. Lett. A **53**, 193 (1975).
[4] C. Taupin, M. Dvolaitzky, and C. Sauterey, Osmotic pressure-induced pores in phospholipid vesicles, Biochemistry **14**, 4771 (1975).
[5] M. M. Koslov and V. S. Markin, A theory of osmotic lysis of lipid vesicles, J. Theor. Biol. **109**, 17 (1984).
[6] S. Olivier, L. Moreaux, and F. Brochard-Wyart, Dynamics of transient pores in stretched vesicles, Proc. Natl. Acad. Sci. **96**, 10591 (1999).
[7] E. Karatekin, S. Olivier, H. Guitouni, N. Borghi, P.-H. Puech, and F. Brochard-Wyart, Cascades of transient pores in giant vesicles: Line tension and transport, Biophys. J. **84**, 1734 (2003).
[8] M. Chabanon, J. C. S. Ho, B. Liedberg, A. N. Parikh, and P. Rangamani, Pulsatile lipid vesicles under osmotic stress, Biophys. J. **112**, 1682 (2017).
[9] Y. Shoji and H. Nakashima, Nutraceutics and delivery systems, J. Drug Target. **12**, 385 (2004).
[10] L. Paasonen, T. Laaksonen, C. Johans, M. Yliperttula, K. Kontturi, and A. Urtti, Gold nanoparticles enable selective light-induced contents release from liposomes, J. Control. Release **122**, 86 (2007).
[11] J. S. Lee and J. Feijen, Polymersomes for drug delivery: Design, formation and characterization, J. Control. Release **161**, 473 (2012).
[12] S. Shin, V. S. Doan, and J. Feng, Osmotic Delivery and Release of Lipid-Encapsulated Molecules Via Sequential Solution Exchange, Phys. Rev. Appl. **12**, 024014 (2019).
[13] M. A. Idiart and Y. Levin, Rupture of a liposomal vesicle, Phys. Rev. E **69**, 061922 (2004).
[14] Y. Levin and M. A. Idiart, Pore dynamics of osmotically stressed vesicles, Phys. A: Stat. Mech. Appl. **331**, 571 (2004).
[15] R. J. Ryham, On the viscous flows of leak-out and spherical cap natation, J. Fluid Mech. **836**, 502 (2017).
[16] W. Helfrich, Elastic properties of lipid bilayers: Theory and possible experiments, Z. Naturforsch. C **28**, 693 (1973).

[17] F. Brochard-Wyart, P.-G. de Gennes, and O. Sandre, Transient pores in stretched vesicles: Role of leak-out, Phys. A: Stat. Mech. Appl. **278**, 32 (2000).

[18] R. Ryham, I. Berezovik, and F. S. Cohen, Aqueous viscosity is the primary source of friction in lipidic pore dynamics, Biophys. J. **101**, 2929 (2011).

[19] C. A. Aubin and R. J. Ryham, Stokes flow for a shrinking pore, J. Fluid Mech. **788**, 228 (2016).

[20] W.-C. Su, D. L. Gettel, M. Chabanon, P. Rangamani, and A. N. Parikh, Pulsatile gating of giant vesicles containing macromolecular crowding agents induced by colligative nonideality, J. Am. Chem. Soc. **140**, 691 (2018).

[21] M. Chabanon and P. Rangamani, Solubilization kinetics determines the pulsatory dynamics of lipid vesicles exposed to surfactant, Biochim. Biophys. Acta (BBA)-Biomembr. **1860**, 2032 (2018).

[22] T. F. Zhu and J. W. Szostak, Exploding vesicles, J. Syst. Chem. **2**, 4 (2011).

[23] A. Peyret, E. Ibarboure, A. Tron, L. Beauté, R. Rust, O. Sandre, N. D. McClenaghan, and S. Lecommandoux, Polymersome popping by light-induced osmotic shock under temporal, spatial, and spectral control, Angew. Chem. Int. Ed. **56**, 1566 (2017).

[24] V. K. Malik, S. Shin, and J. Feng, Light-triggered explosion of lipid vesicles, Soft Matter **16**, 8904 (2020).

[25] U. Seifert, K. Berndl, and R. Lipowsky, Shape transformations of vesicles: Phase diagram for spontaneous-curvature and bilayer-coupling models, Phys. Rev. A **44**, 1182 (1991).

[26] Z. C. Tu and Z. C. Ou-Yang, Recent theoretical advances in elasticity of membranes following helfrich's spontaneous curvature model, Adv. Colloid Interface Sci. **208**, 66 (2014).

[27] H. J. Deuling and W. Helfrich, Red blood cell shapes as explained on the basis of curvature elasticity, Biophys. J. **16**, 861 (1976).

[28] R. Lipowsky, Spontaneous tubulation of membranes and vesicles reveals membrane tension generated by spontaneous curvature, Faraday Discuss. **161**, 305 (2013).

[29] T. Bhatia, S. Christ, J. Steinkühler, R. Dimova, and R. Lipowsky, Simple sugars shape giant vesicles into multispheres with many membrane necks, Soft Matter **16**, 1246 (2020).

[30] P. Wiggins, Life depends upon two kinds of water, PLoS ONE **3**, e1406 (2008).

[31] R. Lipowsky and H.-G. Döbereiner, Vesicles in contact with nanoparticles and colloids, EPL (Europhys. Lett.) **43**, 219 (1998).

[32] B. Różycki and R. Lipowsky, Spontaneous curvature of bilayer membranes from molecular simulations: Asymmetric lipid densities and asymmetric adsorption, J. Chem. Phys. **142**, 054101 (2015).

[33] E. Evans, V. Heinrich, F. Ludwig, and W. Rawicz, Dynamic tension spectroscopy and strength of biomembranes, Biophys. J. **85**, 2342 (2003).

[34] E. Evans and BA Smith, Kinetics of hole nucleation in biomembrane rupture, New J. Phys. **13**, 095010 (2011).

[35] L. Martínez-Balbuena, E. Hernández-Zapata, and I. Santamaría-Holek, Onsager's irreversible thermodynamics of the dynamics of transient pores in spherical lipid vesicles, Eur. Biophys. J. **44**, 473 (2015).

[36] H. Goldstein, C. Poole, and J. Safko, *Classical Mechanics* (Addison-Wesley, San Francisco, 2002).

[37] I. Derényi, F. Jülicher, and J. Prost, Formation and Interaction of Membrane Tubes, Phys. Rev. Lett. **88**, 238101 (2002).

[38] H.-G. Döbereiner, O. Selchow, and R. Lipowsky, Spontaneous curvature of fluid vesicles induced by trans-bilayer sugar asymmetry, Eur. Biophys. J. **28**, 174 (1999).

[39] E. Minguzzi, Rayleigh's dissipation function at work, Eur. J. Phys. **36**, 035014 (2015).

[40] J. T. Jenkins, Static equilibrium configurations of a model red blood cell, J. Math. Biol. **4**, 149 (1977).

[41] S. T. Milner and S. A. Safran, Dynamical fluctuations of droplet microemulsions and vesicles, Phys. Rev. A **36**, 4371 (1987).

[42] W. Rawicz, K. C. Olbrich, T. McIntosh, D. Needham, and E. Evans, Effect of chain length and unsaturation on elasticity of lipid bilayers, Biophys. J. **79**, 328 (2000).

[43] R. Goetz and R. Lipowsky, Computer simulations of bilayer membranes: Self-assembly and interfacial tension, J. Chem. Phys. **108**, 7397 (1998).

[44] W. K. den Otter, Area compressibility and buckling of amphiphilic bilayers in molecular dynamics simulations, J. Chem. Phys. **123**, 214906 (2005).

[45] T. T. Hormel, S. Q. Kurihara, M. K. Brennan, M. C. Wozniak, and R. Parthasarathy, Measuring Lipid Membrane Viscosity Using Rotational and Translational Probe Diffusion, Phys. Rev. Lett. **112**, 188101 (2014).

[46] P. W. Linder, L. R. Nassimbeni, A. Polson, and A. L. Rodgers, The diffusion coefficient of sucrose in water. A physical chemistry experiment, J. Chem. Educ. **53**, 330 (1976).

[47] T. Portet and R. Dimova, A new method for measuring edge tensions and stability of lipid bilayers: Effect of membrane composition, Biophys. J. **99**, 3264 (2010).

[48] E. Evans and D. Needham, Physical properties of surfactant bilayer membranes: Thermal transitions, elasticity, rigidity, cohesion and colloidal interactions, J. Phys. Chem. **91**, 4219 (1987).

[49] K. Olbrich, W. Rawicz, D. Needham, and E. Evans, Water permeability and mechanical strength of polyunsaturated lipid bilayers, Biophys. J. **79**, 321 (2000).

[50] R. M. Venable, F. L. H. Brown, and R. W. Pastor, Mechanical properties of lipid bilayers from molecular dynamics simulation, Chem. Phys. Lipids **192**, 60 (2015).

[51] S. Chakraborty, M. Doktorova, T. R. Molugu, F. A. Heberle, H. L. Scott, B. Dzikovski, M. Nagao, L.-R. Stingaciu, R. F. Standaert, F. N. Barrera, J. Katsaras, G. Khelashvili, M. F. Brown, and R. Ashkar, How cholesterol stiffens unsaturated lipid membranes, Proc. Natl. Acad. Sci. **117**, 21896 (2020).

[52] H. A. Faizi, S. L. Frey, J. Steinkühler, R. Dimova, and P. M. Vlahovska, Bending rigidity of charged lipid bilayer membranes, Soft Matter **15**, 6006 (2019).

[53] S. D. Shoemaker and T. K. Vanderlick, Stress-induced leakage from phospholipid vesicles: Effect of membrane composition, Ind. Eng. Chem. Res. **41**, 324 (2002).

[54] E. Rideau, R. Dimova, P. Schwille, F. R. Wurm, and K. Landfester, Liposomes and polymersomes: A comparative review towards cell mimicking, Chem. Soc. Rev. **47**, 8572 (2018).

[55] S. Pautot, B. J. Frisken, and D. A. Weitz, Engineering asymmetric vesicles, Proc. Natl. Acad. Sci. **100**, 10718 (2003).

[56] K. Kamiya, R. Kawano, T. Osaki, K. Akiyoshi, and S. Takeuchi, Cell-sized asymmetric lipid vesicles facilitate the investigation of asymmetric membranes, Nat. Chem. **8**, 881 (2016).

[57] M. F. Brown, Curvature forces in membrane lipid–protein interactions, Biochemistry **51**, 9782 (2012).

[58] H. Alimohamadi and P. Rangamani, Modeling membrane curvature generation due to membrane–protein interactions, Biomolecules **8**, 120 (2018).

[59] D. Koller and K. Lohner, The role of spontaneous lipid curvature in the interaction of interfacially active peptides with membranes, Biochim. Biophys. Acta (BBA)-Biomembr. **1838**, 2250 (2014).

[60] M. Kisovec, S. Rezelj, P. Knap, M. M. Cajnko, S. Caserman, A. Flašker, N. Žnidaršič, M. Repič, J. Mavri, Y. Ruan, S. Scheuring, M. Podobnik, and G. Anderluh, Engineering a pH responsive pore forming protein, Sci. Rep. **7**, 42231 (2017).